Fabrication and mechanical properties of tungsten carbide thin films via mist chemical vapor deposition

Takumi Ikenoue [a,*], Takuji Yoshida [a], Masao Miyake [a], Ryuta Kasada [b], and Tetsuji Hirato [a]

[a]Graduate School of Energy Science, Kyoto University, Kyoto 606-8501, Japan

[b]Institute for Materials Research, Tohoku University, Sendai 980-8577, Japan

E-mail: ikenoue.takumi.4m@kyoto-u.ac.jp

Abstract

Tungsten carbide thin films are used as wear-resistant coatings. For such applications, it is industrially advantageous to form high-quality thin films on substrates with large areas or complex shapes under atmospheric pressure. Herein, we investigated the feasibility of forming tungsten carbide thin films using a mist chemical vapor deposition method. WC_{1-x} thin films with smooth surfaces were obtained at growth temperatures of 650 °C or above, and the elemental composition ratios of C/W and N/W gradually approached 1 and 0, respectively, with increasing growth temperature. The hardness and Young's modulus of the film obtained at 750 °C were 25 GPa and 409 GPa, respectively. The grown WC_{1-x} films have potential for use as hard coatings.

Keywords: coating materials; thin films; mechanical properties

1. Introduction

Tungsten carbide is known for its advantageous properties, such as its high melting point, high hardness, low friction coefficient, and chemical stability [1–4]. Owing to these excellent mechanical properties, tungsten carbide thin films are used as wear-resistant coatings for mechanical parts, molds, and drilling tools [4,5]. It has also been demonstrated that tungsten carbonitride behaves as an effective diffusion barrier for Cu metallization in semiconductors [6] and as a promising catalyst for hydrazine decomposition [7,8]. Tungsten carbide thin films are typically deposited using various processes, such as physical vapor deposition [9–11] and chemical vapor deposition (CVD) [12–15]. CVD is a major method for fabricating highly dense, pure films with good uniformity and adhesion. From the perspective of applying tungsten carbide as a coating, the CVD method is considered optimal because it allows for high-quality film formation onto substrates with large areas or complex shapes. However, almost all conventional CVD methods are vacuum processes and consequently require large and expensive vacuum systems and consume large amounts of energy. There are some CVD methods that are capable of fabricating thin films under atmospheric pressure, but they ultimately require a complex and expensive system, such as a plasma generator.

The mist CVD method is receiving increasing attention as a promising technique for the deposition of thin films under atmospheric pressure using a source material solution [16–22]. One of the main advantages is that it is not always necessary to use volatile precursors in mist CVD; therefore, there is a wider choice of precursors and fewer chemical-compound-related limitations. Thus, mist CVD is an industrially advantageous method for the fabrication of thin films. Earlier studies have mainly applied mist CVD to the preparation of oxide films, such as ZnO [16–18], Ga_2O_3 [19,20], Cu_2O [21,22], and NiO [23]. Additionally, sulfide thin films, such as ZnS [24,25] and Cu_2ZnSnS_4 [26], and all-inorganic halide perovskite [27] thin films have been fabricated by this method. However, there have been no reports on the growth of carbides or nitrides using the mist CVD method.

In this study, we investigated the feasibility of forming tungsten carbide thin films using mist CVD. We performed mist CVD under atmospheric pressure at various temperatures using an acetonitrile (CH_3CN) solution containing a tungsten salt as the source solution. The composition and phase of the resulting films were investigated. Furthermore, the hardness and elastic modulus of the films were examined by nanoindentation.

2. Experimental

2.1. Formation of tungsten carbide thin films via mist CVD.

A schematic diagram of the mist CVD system is shown in Fig. 1. Briefly, a liquid solution containing source materials is atomized by an ultrasonic generator, and the formed mist particles are transferred with a carrier gas to the substrate, which is thermally heated. The films are then grown essentially by the CVD mechanism. Details on the mist CVD method can be found in the literature [18–20,28,29]. In this study, a similar system was used, but with the addition of a mist collection trap as shown in Fig. 1. The mist particles that have passed through the tubular furnace are collected by passing through the collection trap, which is filled with the same solvent as the source solution. This collection trap helps not only to collect the mist particles but also to reduce the oxygen partial pressure (preventing backflow of oxygen) and prevents spontaneous combustion of the high-temperature solvent.

For the tungsten carbide thin film growth, the source solution was prepared by dissolving WCl_6 as the W source in acetonitrile as the C source at a concentration of 0.05 mol L^{-1}. An Ar-5%H_2 mixture was used as the carrier gas and dilution gas at flow rates of 4.0 and 2.0 L min^{-1}, respectively. Quartz and alumina substrates (25 mm × 25 mm × 0.7 mm) were used. The growth temperature of tungsten carbide was set in the range of 550 to 850 °C. When the film was formed at high temperatures above 750 °C on the quartz substrate, cracking or peeling due to the difference in thermal expansion coefficients between the film (5.2×10^{-6} K^{-1}) and the quartz substrate (0.6×10^{-6} K^{-1}) occurred. Therefore, the alumina substrate (8.0×10^{-6} K^{-1}) was used for film formation for nanoindentation tests.

2.2. Characterization.

The phase of the obtained films was determined using X-ray diffraction (XRD; X'pertPRO-MPD with Cu Kα radiation, λ = 0.15406 nm). The morphology of the films was observed by scanning electron microscopy (SEM; JSM-6510LV, JEOL) and field-emission SEM (FE-SEM, SU6600, Hitachi High-Technologies). The composition of the films was determined by X-ray photoelectron spectroscopy (XPS; JPS-9030, JEOL) and energy dispersive spectroscopy (EDS; INCAx-act, Oxford Instruments). XPS was also used to identify the chemical bonding states of the elements of the films.

The mechanical properties (hardness and Young's modulus) of the films were determined by nanoindentation using Nanoindenter G200 (Agilent Technologies) with a three-sided pyramidal Berkovich indenter tip [30]. Continuous stiffness measurements (CSMs) were carried out under the following conditions: depth limit of 2000 nm, targeted

strain rate of 0.05 s^{-1}, and targeted frequency of 45 Hz. This method is capable of obtaining hardness and Young's modulus as a continuous function of indentation depth. Twelve measurements were made on each sample. Each measurement point was separated by at least 100 μm from all other measurement points. For the calculations of hardness and Young's modulus, the Poisson's ratio of the films was assumed to be 0.18 [31].

To inspect the phenomena occurring in the films during CSMs, a standard constant strain rate (CSR) test was performed with various indentation depth limits (25–1000 nm) at a targeted strain rate of 0.05 s^{-1}; the morphology of the indentation was then observed with SEM.

3. Results and Discussion

3.1. Composition and morphology.

No films were obtained at growth temperatures below 650 °C. The appearances of the thin films obtained at each growth temperature are shown in Fig. 2. The films obtained at 650–750 °C exhibited a metallic luster (Fig. 2a–c, f). This luster faded as the growth temperature increased beyond 750 °C (Fig. 2d) and did not occur for the film deposited at 850 °C (Fig. 2e).

The surface SEM images of the films are shown in Fig. 3. The films deposited at 650–750 °C have smooth surfaces (Fig. 3a–c), which is expected based on their metallic luster. In contrast, many particles with diameters of 1–3 μm were observed on the surfaces of the films deposited at 800 and 850 °C (Fig. 3d and e). The films deposited at 650–750 °C should be favorable for wear-resistant coatings because a low friction coefficient can be expected from the smooth surfaces.

Figure 4 shows the cross-sectional SEM images of the films. Whereas the film deposited at 850 °C is composed of loosely packed coarse grains, the films deposited at lower temperatures are dense. The thickness of the films tends to increase with increasing growth temperature, from 500 nm at 650 °C to 1260 nm at 800 °C.

The compositions of the obtained films were evaluated by XPS and EDS analysis. Fig. 5 (a) shows XPS wide scan spectra of each sample. Only the peaks of tungsten, carbon, nitrogen, and chlorine, derived from the precursor, and oxygen, as impurities derived from the atmosphere, were detected. In all samples, pronounced peaks derived from oxygen, which are considered to be surface oxide layers (WO_3) formed due to exposure to the atmosphere, were detected from the outermost surface. The peaks derived from these surface oxide layers almost disappeared upon argon etching for about 1 minute. Fig. 5 (b) shows the results of XPS depth direction quantitative analysis of the sample obtained

at 650 °C. Except for the outermost surface, the film was essentially formed of tungsten and carbon with slight amounts of oxygen, nitrogen, and chlorine. The composition was almost constant in the depth direction and almost coincided with the result of the quantitative analysis by EDS. The elemental content ratios of C/W and N/W of the films analyzed by EDS are plotted against the growth temperature in Fig. 6. As the growth temperature increases, the C/W and N/W ratios decrease asymptotically to 1 and 0, respectively, which correspond to the WC stoichiometric values. The film obtained at 850 °C has a particularly high C/W ratio. We speculate that the film contains amorphous carbon (a-C), similar to a previously reported WN_xC_y film formed at a high temperature by aerosol-assisted CVD [32]. The columnar structure seen in the SEM image of the film obtained at 850 °C (Fig. 4e) is thought to be this co-deposited a-C. This is also suggested by the XPS C 1s BE narrow scans of the samples obtained at each temperature, as shown in Fig. 5 (c). In the spectra, three types of carbon were observed via the peaks at 283.4, 284.3, and 285.7 eV, which were assigned to WC, graphitic, and C-OH bonds, respectively. These values for the C 1s peak agrees well with the reported values of 284.2–285.2 and 279.7–283.8 eV for amorphous C and WC, respectively [33,34]. In particular, the peak intensity derived from amorphous C was significantly increased in the film obtained at 850 °C, suggesting the formation of amorphous C.

The XRD patterns of the obtained thin films on alumina and quartz substrates at various growth temperatures are presented in Fig. 7. Broad peaks corresponding to cubic WC_{1-x} (ICDD ref. code: 00-020-1316) are present in the pattern of the films deposited at 650 °C and at higher temperatures, whereas no peaks except for those of the substrate are present for a growth temperature of 550 °C, at which no film was obtained. Similar XRD peaks for WC_{1-x} are present between the films obtained on alumina and quartz substrates. Therefore, the crystal structure of tungsten carbide does not depend on the substrate. WC_{1-x} exists as a thermodynamically stable phase at a high temperature of approximately 2500 °C [1]. However, it has been reported that WC_{1-x} can also be obtained at low temperatures by magnetron sputtering [10]. Although the detailed cause has not been elucidated, it is thought that the WC_{1-x} observed in this study was obtained via a similar mechanism, even when using the mist CVD method.

The fabrication of WC_{1-x} thin films by mist CVD was successful at growth temperatures of 650 °C and above. WC_{1-x} films with smooth surfaces were obtained at 650–750 °C that are expected to be suitable for use as wear-resistant coatings.

3.2. Mechanical properties.

The hardness-displacement curves, Young's modulus-displacement curves, and load-

displacement curves from CSMs of the WC_{1-x} thin films deposited at 650 and 750 °C on alumina substrates are shown in Fig. 8. From Fig. 8a and b, both the hardness and Young's modulus of the film deposited at 650 °C are nearly constant in the displacement range of 250–450 nm. In this range, the mechanical properties of the film were accurately measurable. On the other hand, in the shallow displacement region, peaks at approximately 80 nm occurred in each profile. In this shallow displacement region, elastic deformation of the film caused by the spherical tip of the indenter dominates over plastic deformation [35] or so-called indentation size effects with an artifact in the CSM appeared [36], which results in the observed profile peak shape. At displacements larger than 450 nm, the hardness and Young's modulus decrease gradually to a constant value. This suggests that the influence of the substrate emerges when the displacement is near the thickness of the film (approximately 500 nm in this case). Notably, in the load-displacement curve shown in Fig. 8c, there is a region where the displacement changes, while the load is constant. The effect in this region will be described later with the results of the CSR tests.

Based on the above, the hardness and Young's modulus of the film deposited at 650 °C were determined as 17 GPa and 301 GPa, respectively, at a displacement of 300 nm, where the substrate did not affect the results. The hardness and Young's modulus curves of the film deposited at 750 °C (Fig. 8d and e) show the same tendency as those of the film deposited at 650 °C. In the same way, the hardness and Young's modulus of this film were determined to be 25 GPa and 409 GPa, respectively, at a displacement of 700 nm. This result shows that the WC_{1-x} thin films deposited via mist CVD have mechanical properties equal to or higher than that of tungsten carbide thin films prepared by vacuum processes, such as magnetron sputtering [2].

The surface of the film deposited at 850 °C was very rough, where cracks tended to propagate along grain boundaries, which allowed the tip of the indenter to penetrate the film at a small load. Therefore, the film was broken instead of experiencing plastic deformation, and thus the mechanical properties could not be measured accurately.

To reveal what kind of phenomena occurred in the film at each displacement, especially the displacement equivalent to the film thickness, CSR tests on the film deposited at 650 °C on alumina were performed with various depth limits, and the impressions were observed with SEM. The surface morphology of the impression for a maximum displacement of 320 nm is shown in Fig. 9a. The triangle impression was left by the Berkovich indenter tip without fracturing the film. For the geometry of the Berkovich indenter tip, the length of one side of the residual impression is 7.5 times the indentation depth [37]. For a displacement of 320 nm, the set indentation depth is in good agreement

with the indentation depth estimated from the size of the impression. This means that the mechanical properties can be accurately evaluated in this displacement region.

Figure 9b shows the surface morphology of the impression at a maximum displacement of 429 nm. The shape of this impression is not triangular, and its size is much larger than the expected size based on the penetration depth. This result suggests that film cracks and delamination occur around and under the indenter tip before it reaches a displacement of 429 nm.

The load-displacement CSR curves for the WC_{1-x} thin film deposited at 650 °C on alumina are shown in Fig. 10. The load-displacement curve with a depth limit of 300 nm (Fig. 10a) has a general shape, whereas in that for a depth limit of 350 nm (Fig. 10b), the displacement changes from approximately 350 nm by approximately 100 nm at a constant load of 22 mN. In general, such a change in the load-displacement curve is associated with through-thickness fracture of the coating, delamination of the coating, or even nucleation of plasticity in the underlying substrate [35]. Considering the observed CSR impressions (Fig. 9), the load-displacement curves suggest that cracks or delamination occurred in the film at a 350-nm displacement, and thus the displacement greatly increased, while the load remained constant at 22 mN.

In the load-displacement curve (Fig. 8c) described above, there is a region where the displacement changes at a constant load. As indicated by the CSR tests, cracks or delamination are considered to occur in this range, and thus the mechanical properties cannot be measured accurately. Therefore, the values at displacements shallower than this region with a nearly constant hardness and Young's modulus were determined as the mechanical characteristics of the film.

The mechanical properties of the WC_{1-x} thin films were evaluated by nanoindentation (CSM). The film deposited at 750 °C has a hardness of 25 GPa and Young's modulus of 409 GPa. These results demonstrate that the WC_{1-x} thin film deposited by mist CVD has a hardness comparable to that of films deposited by other deposition methods with vacuum systems.

4. Conclusion

WC_{1-x} thin films with smooth surfaces were obtained by the mist CVD method. The WC_{1-x} thin films were obtained at growth temperatures of 650 °C and above, and the elemental composition ratios of C/W and N/W gradually approached the stoichiometric ratio with increasing growth temperature. The hardness and Young's modulus of the film obtained at 750 °C were 25 GPa and 409 GPa, respectively. These grown WC_{1-x} films thus have potential for use as hard coatings.

Acknowledgments

This work was supported by the JSPS Grant-in-Aid for Challenging Exploratory Research [grant number JP15K14181].

Declarations of interest: none.

References

[1] A.S. Kurlov, A.I. Gusev, Tungsten carbides and W-C phase diagram, Inorg. Mater. 42 (2006) 121–127. doi:10.1134/S0020168506020051.

[2] K. Abdelouahdi, C. Sant, C. Legrand-Buscema, P. Aubert, J. Perrière, G. Renou, P. Houdy, Microstructural and mechanical investigations of tungsten carbide films deposited by reactive RF sputtering, Surf. Coatings Technol. 200 (2006) 6469–6473. doi:10.1016/j.surfcoat.2005.11.015.

[3] J.E. Krzanowski, J.L. Endrino, The effects of substrate bias on phase stability and properties of sputter-deposited tungsten carbide, Mater. Lett. 58 (2004) 3437–3440. doi:10.1016/j.matlet.2004.04.036.

[4] J. Esteve, G. Zambrano, C. Rincon, E. Martinez, H. Galindo, P. Prieto, Mechanical and tribological properties of tungsten carbide sputtered coatings, Thin Solid Films. 373 (2000) 282–286. doi:10.1016/S0040-6090(00)01108-1.

[5] D. Garg, P.N. Dyer, D.B. Dimos, S. Sunder, H.E. Hintermann, M. Maillat, Low-Temperature Chemical Vapor Deposition Tungsten Carbide Coatings for Wear/Erosion Resistance, J. Am. Ceram. Soc. 75 (1992) 1008–1011. doi:10.1111/j.1151-2916.1992.tb04176.x.

[6] S.J. Wang, H.Y. Tsai, S.C. Sun, Characterization of Tungsten Carbide as Diffusion Barrier for Cu Metallization, Jpn. J. Appl. Phys. 40 (2001) 2642–2649. doi:10.1143/JJAP.40.2642.

[7] J. Santos, Catalytic Decomposition of Hydrazine on Tungsten Carbide: The Influence of Adsorbed Oxygen, J. Catal. 210 (2002) 1–6. doi:10.1006/jcat.2002.3634.

[8] J. Sun, M. Zheng, X. Wang, A. Wang, R. Cheng, T. Li, T. Zhang, Catalytic Performance of Activated Carbon Supported Tungsten Carbide for Hydrazine Decomposition, Catal. Letters. 123 (2008) 150–155. doi:10.1007/s10562-008-9409-5.

[9] E. Raekelboom, K. Abdelouahdi, C. Legrand-Buscema, Structural investigation by the Rietveld method of sputtered tungsten carbide thin films, Thin Solid Films. 517 (2009) 1555–1558. doi:10.1016/j.tsf.2008.09.085.

[10] E.C. Weigert, M.P. Humbert, Z.J. Mellinger, Q. Ren, T.P. Beebe, L. Bao, J.G. Chen, Physical vapor deposition synthesis of tungsten monocarbide (WC) thin films on different carbon substrates, J. Vac. Sci. Technol. A Vacuum, Surfaces, Film. 26 (2008) 23–28. doi:10.1116/1.2806941.

[11] G. Keller, I. Barzen, R. Erz, W. Dötter, S. Ulrich, K. Jung, H. Ehrhardt, Crystal structure, morphology and composition of magnetron sputtered tungsten carbide films, Fresenius. J. Anal. Chem. 341 (1991) 349–352. doi:10.1007/BF00321934.

[12] K.A. Beadle, R. Gupta, A. Mathew, J.G. Chen, B.G. Willis, Chemical vapor deposition of phase-rich WC thin films on silicon and carbon substrates, Thin Solid Films. 516 (2008) 3847–3854. doi:10.1016/j.tsf.2007.06.170.

[13] A. Jafari, R. Alipour, M. Ghoranneviss, A.H. Ramezani, Specialized Study on Morphological Features of Tungsten Carbide Thin Film Synthesis by HFCVD, J. Inorg. Organomet. Polym. Mater. 26 (2016) 384–393. doi:10.1007/s10904-016-0328-4.

[14] K.K. Lai, H.H. Lamb, Precursors for Organometallic Chemical Vapor Deposition of Tungsten Carbide Films, Chem. Mater. 7 (1995) 2284–2292. doi:10.1021/cm00060a016.

[15] M.A. Neto, E.L. Silva, A.J.S. Fernandes, F.J. Oliveira, R.F. Silva, Deposition of alpha-WC/a-C nanocomposite thin films by hot-filament CVD, Surf. Coatings Technol. 206 (2011) 103–106. doi:10.1016/j.surfcoat.2011.06.049.

[16] H. Nishinaka, T. Kawaharamura, S. Fujita, Low-Temperature Growth of ZnO Thin Films by Linear Source Ultrasonic Spray Chemical Vapor Deposition, Jpn. J. Appl. Phys. 46 (2007) 6811–6813. doi:10.1143/JJAP.46.6811.

[17] T. Kawaharamura, H. Nishinaka, S. Fujita, Growth of Crystalline Zinc Oxide Thin Films by Fine-Channel-Mist Chemical Vapor Deposition, Jpn. J. Appl. Phys. 47 (2008) 4669–4675. doi:10.1143/JJAP.47.4669.

[18] H. Nishinaka, Y. Kamada, N. Kameyama, S. Fujita, Epitaxial ZnO Thin Films on a -Plane Sapphire Substrates Grown by Ultrasonic Spray-Assisted Mist Chemical Vapor Deposition, Jpn. J. Appl. Phys. 48 (2009) 121103. doi:10.1143/JJAP.48.121103.

[19] D. Shinohara, S. Fujita, Heteroepitaxy of Corundum-Structured α-Ga 2 O 3 Thin Films on α-Al 2 O 3 Substrates by Ultrasonic Mist Chemical Vapor Deposition, Jpn. J. Appl. Phys. 47 (2008) 7311–7313. doi:10.1143/JJAP.47.7311.

[20] K. Akaiwa, S. Fujita, Electrical Conductive Corundum-Structured $¥alpha$-Ga$_{2}$O$_{3}$ Thin Films on Sapphire with Tin-Doping Grown by Spray-Assisted Mist Chemical Vapor Deposition, Jpn. J. Appl. Phys. 51 (2012) 070203. doi:10.1143/JJAP.51.070203.

[21] T. Ikenoue, S. Sakamoto, Y. Inui, Fabrication and characteristics of p-type Cu 2 O thin films by ultrasonic spray-assisted mist CVD method, Jpn. J. Appl. Phys. 53 (2014) 05FF06. doi:10.7567/JJAP.53.05FF06.

[22] T. Ikenoue, T. Kawai, R. Wakashima, M. Miyake, T. Hirato, Hole mobility improvement in Cu 2 O thin films prepared by the mist CVD method, Appl. Phys. Express. 12 (2019) 055509. doi:10.7567/1882-0786/ab15b3.

[23] T. Ikenoue, J. Inoue, M. Miyake, T. Hirato, Epitaxial growth of undoped and Li-

doped NiO thin films on α-Al2O3 substrates by mist chemical vapor deposition, J. Cryst. Growth. 507 (2019) 379–383. doi:10.1016/j.jcrysgro.2018.11.032.

[24] K. Uno, Y. Yamasaki, P. Gu, I. Tanaka, Growth of zinc sulfide by mist chemical vapor deposition depending on mist size and thermal conditions in susceptor, Phys. Status Solidi. 13 (2016) 448–451. doi:10.1002/pssc.201510309.

[25] K. Uno, Y. Yamasaki, I. Tanaka, Growth mechanisms of zinc oxide and zinc sulfide films by mist chemical vapor deposition, Appl. Phys. Express. 10 (2017) 015502. doi:10.7567/APEX.10.015502.

[26] K. SHIBAYAMA, K. KANEKO, S. FUJITA, Fabrication of Cu_2ZnSnS_4 Thin Films by Ultrasonic-Atomized Mist Methods, J. Soc. Mater. Sci. Japan. 64 (2015) 410–413. doi:10.2472/jsms.64.410.

[27] Y. Haruta, T. Ikenoue, M. Miyake, T. Hirato, Fabrication of (101)-oriented CsPbBr 3 thick films with high carrier mobility using a mist deposition method, Appl. Phys. Express. 12 (2019) 085505. doi:10.7567/1882-0786/ab2c96.

[28] H. Nishinaka, Y. Kamada, N. Kameyama, S. Fujita, Growth characteristics of single-crystalline ZnMgO layers by ultrasonic spray assisted mist CVD technique, Phys. Status Solidi. 247 (2010) 1460–1463. doi:10.1002/pssb.200983247.

[29] N. Suzuki, K. Kaneko, S. Fujita, Growth of corundum-structured In2O3 thin films on sapphire substrates with Fe2O3 buffer layers, J. Cryst. Growth. 364 (2013) 30–33. doi:10.1016/j.jcrysgro.2012.11.065.

[30] W.C. Oliver, G.M. Pharr, An improved technique for determining hardness and elastic modulus using load and displacement sensing indentation experiments, J. Mater. Res. 7 (1992) 1564–1583. doi:10.1557/JMR.1992.1564.

[31] H.L. Brown, P.E. Armstrong, C.P. Kempter, Elastic Properties of Some Polycrystalline Transition - Metal Monocarbides, J. Chem. Phys. 45 (1966) 547–549. doi:10.1063/1.1727602.

[32] D. Kim, O.H. Kim, T. Anderson, J. Koller, L. McElwee-White, L.-C. Leu, J.M. Tsai, D.P. Norton, Chemical vapor deposition of WNxCy using the tungsten piperidylhydrazido complex Cl4(CH3CN)W(N-pip): Deposition, characterization, and diffusion barrier evaluation, J. Vac. Sci. Technol. A Vacuum, Surfaces, Film. 27 (2009) 943–950. doi:10.1116/1.3106625.

[33] J. Luthin, C. Linsmeier, Influence of oxygen on the carbide formation on tungsten, J. Nucl. Mater. 290–293 (2001) 121–125. doi:10.1016/S0022-3115(00)00429-3.

[34] R.J. Colton, J.W. Rabalais, Electronic structure to tungsten and some of its borides, carbides, nitrides, and oxides by x-ray electron spectroscopy, Inorg. Chem. 15 (1976) 236–238. doi:10.1021/ic50155a049.

[35] S.J. Bull, Nanoindentation of coatings, J. Phys. D. Appl. Phys. 38 (2005) R393–R413. doi:10.1088/0022-3727/38/24/R01.

[36] G.M. Pharr, J.H. Strader, W.C. Oliver, Critical issues in making small-depth mechanical property measurements by nanoindentation with continuous stiffness measurement, J. Mater. Res. 24 (2009) 653–666. doi:10.1557/jmr.2009.0096.

[37] A.C. Fischer-Cripps, Nanoindentation, Springer New York, New York, NY, 2011. doi:10.1007/978-1-4419-9872-9.

Fabrication and mechanical properties of tungsten carbide thin films via mist chemical vapor deposition: Highlights

- Smooth tungsten carbide thin films prepared at atmospheric pressure and 650–750 °C
- Mechanical properties equal to or higher than those obtained via vacuum processes
- Hardness and Young's modulus for 750 °C film of 25 GPa and 409 GPa, respectively

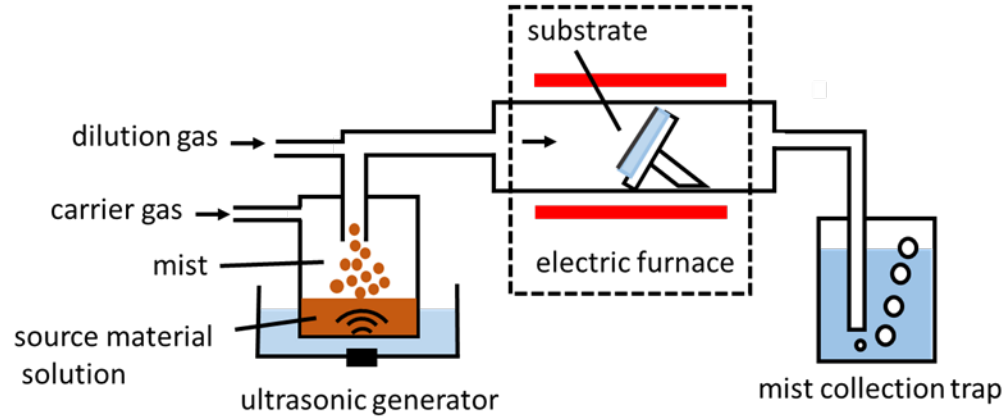

Fig. 1 Schematic of the mist CVD system.

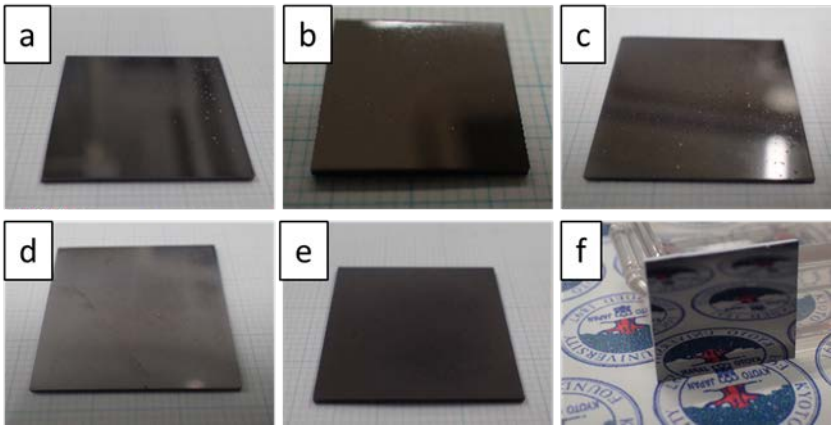

Fig. 2 Appearances of tungsten carbide films obtained at (a) 650 °C, (b) 700 °C, (c) 750 °C, (d) 800 °C, and (e) 850 °C on alumina substrates. A typical film surface with a metallic luster is shown in (f).

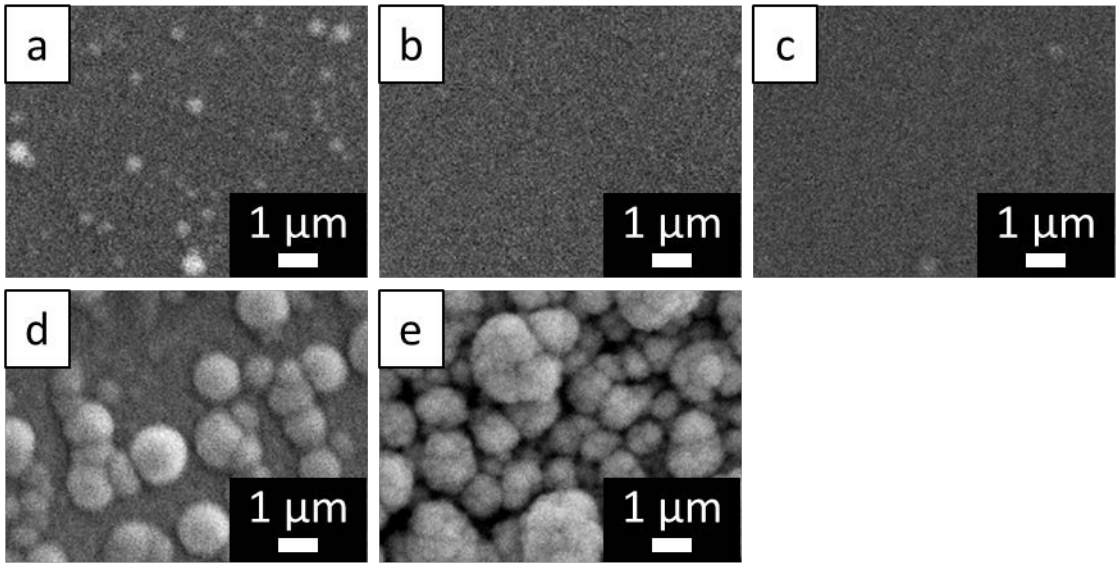

Fig. 3 Surface SEM images of tungsten carbide films obtained at (a) 650 °C, (b) 700 °C, (c) 750 °C, (d) 800 °C, and (e) 850 °C on alumina substrates.

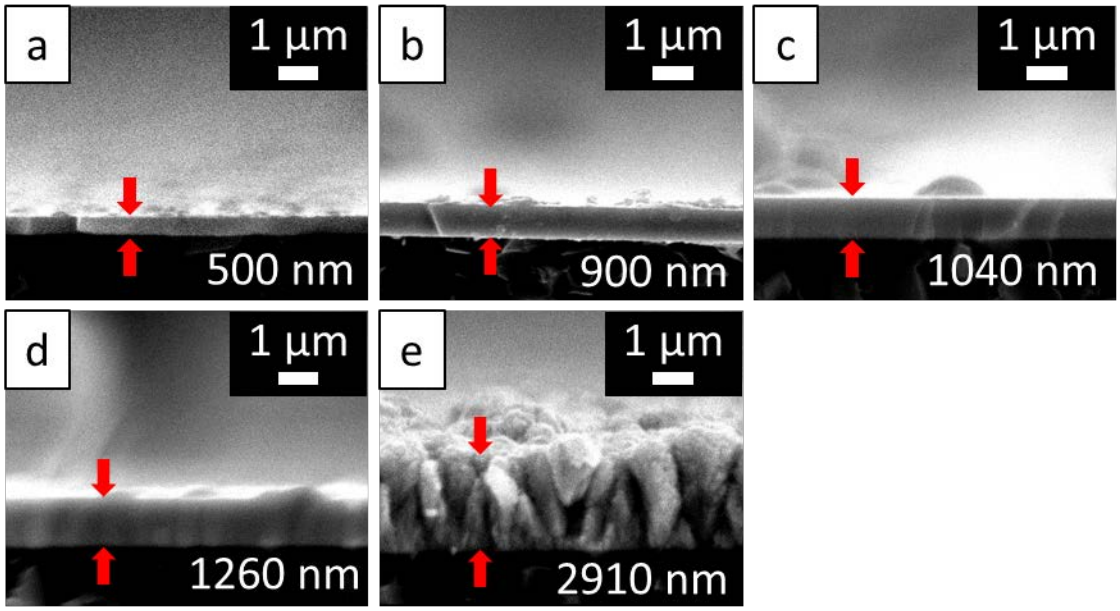

Fig. 4 Cross-sectional SEM images of tungsten carbide films obtained at (a) 650 °C, (b) 700 °C, (c) 750 °C, (d) 800 °C, and (e) 850 °C on alumina substrates.

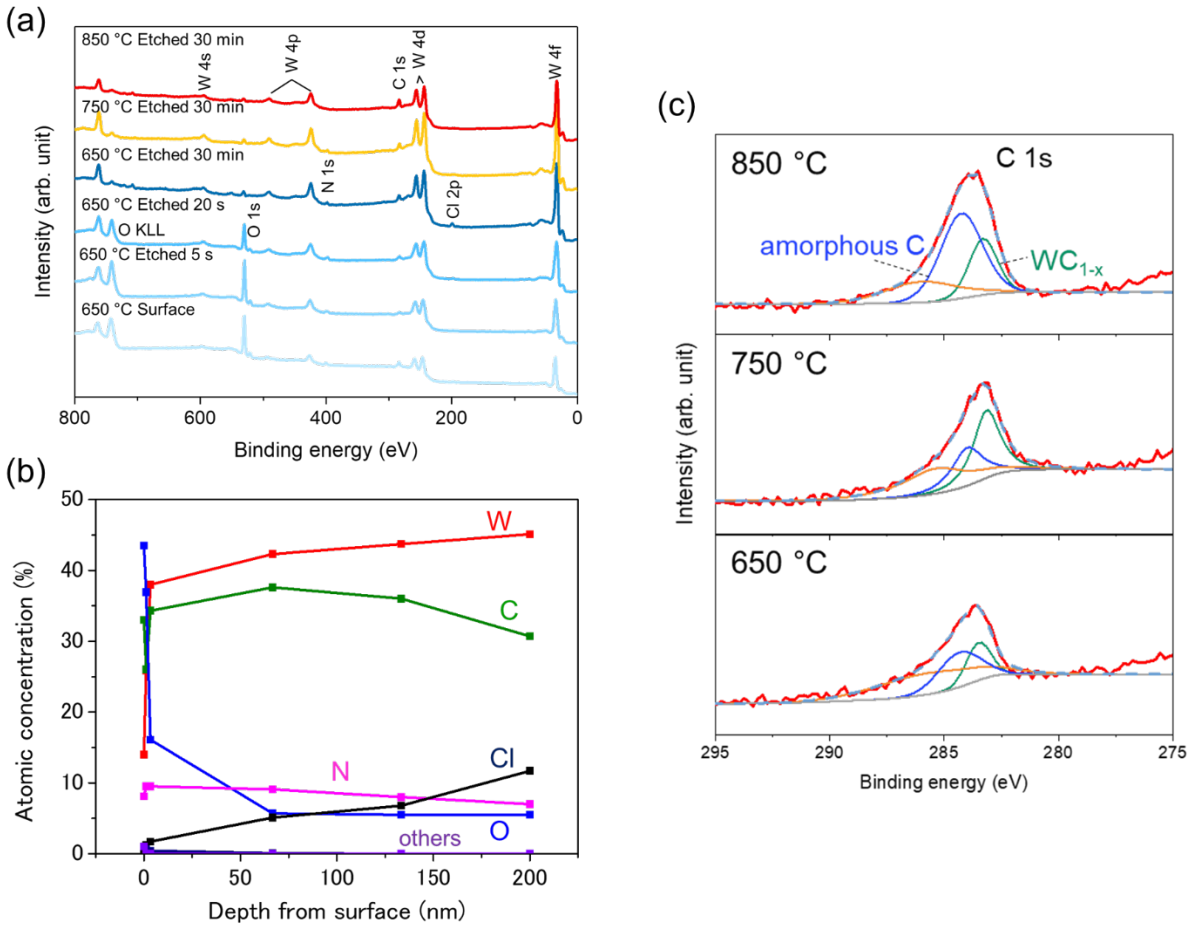

Fig. 5 (a) XPS wide scan spectra of the tungsten carbide films obtained at 650–850 °C, (b) quantitative XPS depth profile of the films obtained at 650 °C, and (c) XPS narrow scan spectra of the C1s region for the films obtained at 650–850 °C.

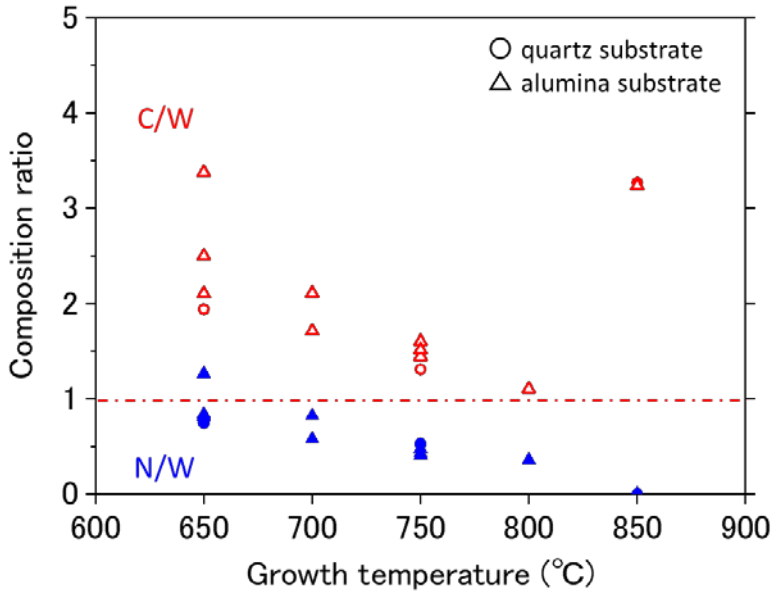

Fig. 6 Elemental composition ratios of C/W (red open symbols) and N/W (blue solid symbols) in the films on quartz and alumina substrates as a function of growth temperature.

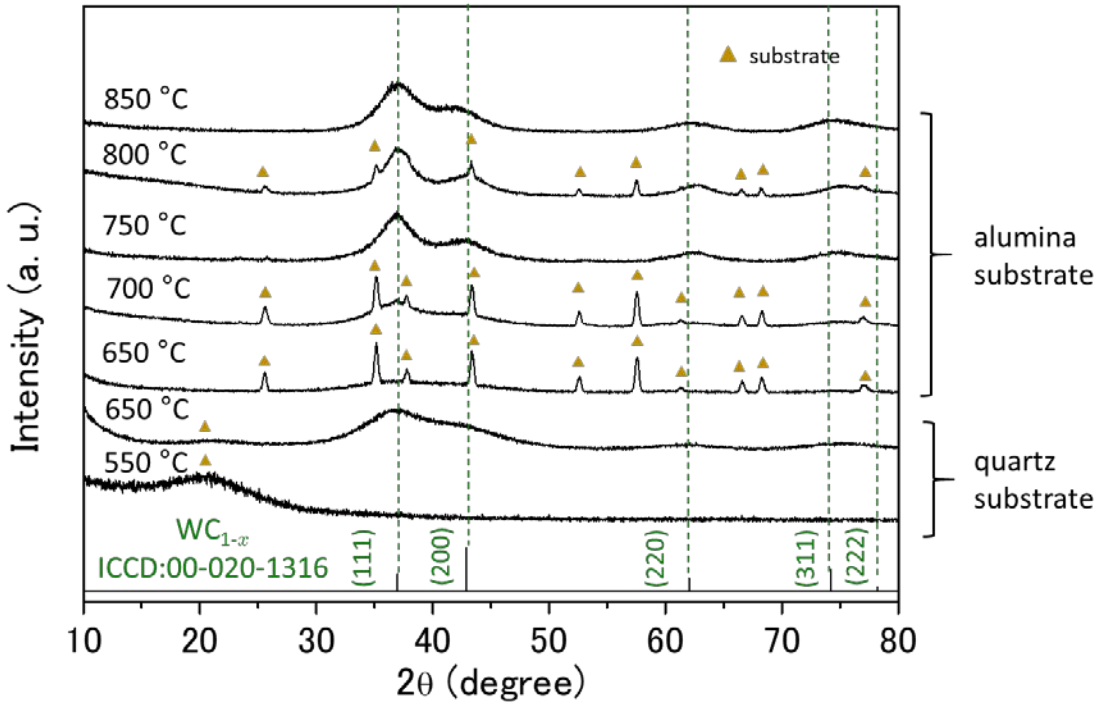

Fig. 7 XRD patterns of obtained films on alumina or quartz substrates at various growth temperatures.

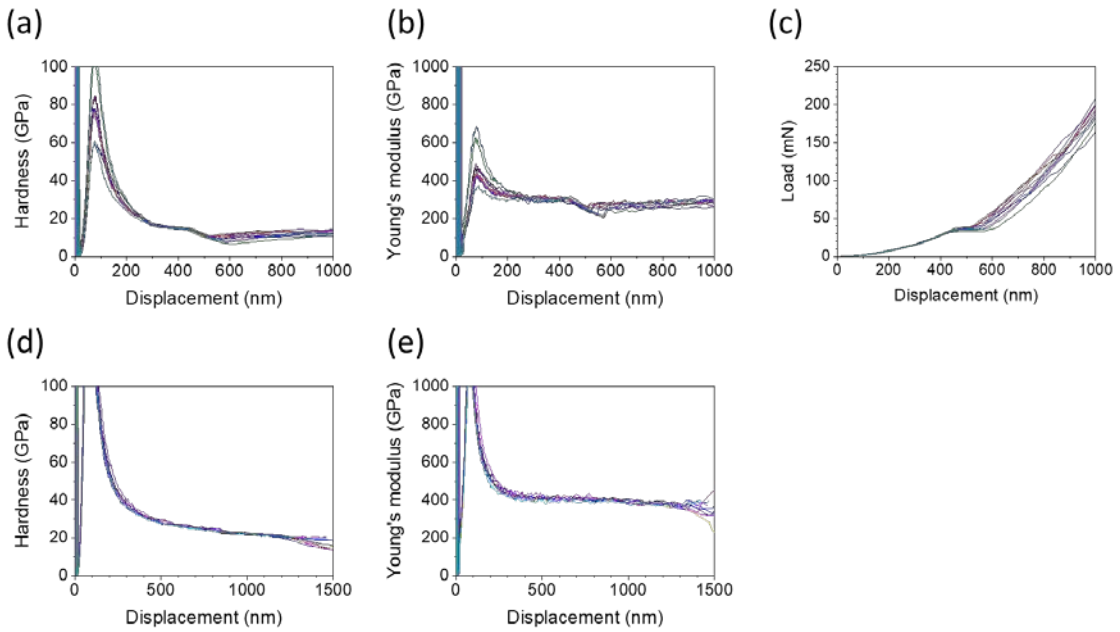

Fig. 8 Hardness-displacement curves, Young's modulus-displacement curves, and load-displacement curves from CSMs of WC_{1-x} films obtained at (a-c) 650 °C and (d,e) 750 °C on alumina substrates.

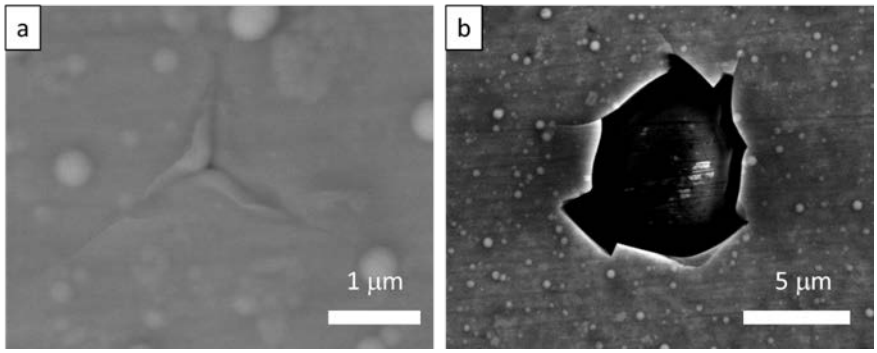

Fig. 9 Morphology of impressions from CSR testing on WC_{1-x} thin films obtained at 650 °C on alumina. The maximum displacements are (a) 320 nm and (b) 429 nm.

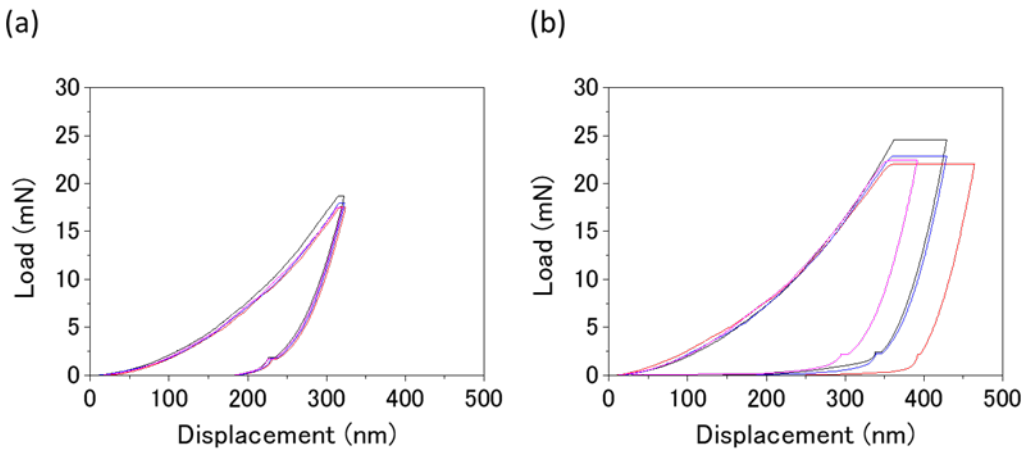

Fig. 10 Load-displacement curves from CSR tests of WC_{1-x} thin films deposited at 650 °C on alumina. The set depth limits are (a) 300 nm and (b) 350 nm.